# Growth of Au–$TiO_2$ nanocomposite thin films by a dual-laser, dual-target system

E. György,[a] G. Sauthier, and A. Figueras
*Consejo Superior de Investigaciones Científicas, Instituto de Ciencia de Materiales, Campus UAB, 08193 Bellaterra, Spain*

A. Giannoudakos[b] and M. Kompitsas
*Theoretical and Physical Chemistry Institute, National Hellenic Research Foundation, Vasileos Konstantinou Avenue 48, 11635 Athens, Greece*

I. N. Mihailescu
*National Institute for Lasers, Plasma and Radiations Physics, P.O. Box MG 36, 77125 Bucharest, Romania*

(Received 20 July 2006; accepted 15 September 2006; published online 1 December 2006)

Nanocomposite thin films formed by gold nanoparticles embedded in a titanium dioxide matrix have been synthesized by pulsed laser deposition. Two synchronized laser sources, an $ArF^*$ excimer ($\lambda = 193$ nm, $\tau_{FWHM} \sim 12$ ns) laser and a frequency tripled Nd:yttrium aluminium garnet ($\lambda = 355$ nm, $\tau_{FWHM} \sim 10$ ns) laser, were used for the simultaneous ablation of the titanium dioxide and gold targets. The optical absorption characteristics of the obtained nanocomposites were investigated as a function of laser parameters used for the ablation of the gold target. The obtained results proved the possibility of tuning the optical properties of gold–titanium dioxide nanocomposites with the proper choice of laser irradiation parameters. Band gap narrowing and absorption in the visible spectral region induced by the incorporation of gold enable the design of nanostructured thin films to be achieved for photocatalysts and solar energy converters.
 [DOI: 10.1063/1.2372450]

## I. INTRODUCTION

Titanium dioxide ($TiO_2$) thin films have received significant attention during recent years due to their photocatalytic and optoelectronic properties. $TiO_2$ crystallizes in three different structures: rutile, anatase, and brookite. Among these phases anatase is known for its higher photocatalytic performances and is used in a large field of technology applications such as deodorizing, air and water treatment, and gas and organic compound decomposition. In addition, its photoinduced hydrophobic to hydrophilic conversion makes it appropriate for antifogging and self-cleaning products.[1,2] Nevertheless, anatase is thermodynamically not as stable as rutile, the most common $TiO_2$ crystal phase in nature. Thus, the synthesis of pure anatase phase $TiO_2$ thin films is quite difficult.

Furthermore, due to its relatively large band gap (3.2 eV) $TiO_2$ absorbs only a small fraction of the solar radiation (the UV component). Significant research has been focused on the development of a generation of $TiO_2$ photocatalysts to overcome this shortcoming through the identification of possible solutions for extending the absorption range in the visible light spectrum. Such attempts include doping of the $TiO_2$ host material with nonmetal[3] or metal ions,[4–6] as well as partial coating with metals.[7,8]

Different methods have been used for the preparation of $TiO_2$ thin films, such as chemical vapor deposition,[9] magnetron sputtering,[10,11] sol-gel chemistry,[12] thermal oxidation,[13] or direct laser irradiation[14] of Ti metal surfaces, as well as pulsed lased deposition (PLD).[15–17] When compared with other techniques, PLD has the advantage of precise and simultaneous control of stoichiometry, crystalline status, and thickness of the growing thin films through the experimental process parameters.

In this paper we report on the synthesis and characterization of Au–$TiO_2$ nanocomposite thin films prepared by PLD using a dual-laser, dual-target system. We show that the two-laser PLD method enables the continuous tuning of the amount of Au in the $TiO_2$ thin films through the laser fluence incident on the Au target, which in turn determines the optical properties of the synthesized nanocomposite materials in the near-UV and visible spectral regions.

## II. EXPERIMENTAL DETAILS

The deposition of the Au–$TiO_2$ nanostructures was performed inside a stainless steel vacuum chamber. Prior to each irradiation the vacuum chamber was evacuated down to a residual pressure of $7 \times 10^{-4}$ Pa. For the host $TiO_2$ target ablation we applied UV laser pulses generated by a Lumonics model TE-861T $ArF^*$ excimer laser ($\lambda = 193$ nm, $\tau_{FWHM} \sim 12$ ns). For ablation of the Au targets we used the pulses from a Quantel model YG851 Nd:YAG (yttrium aluminum garnet) laser ($\lambda = 355$ nm, $\tau_{FWHM} \sim 10$ ns). The two lasers were synchronized and operated at 10 Hz pulse repetition rate. The incidence angle of the beams was about 30° relative to the normal of the target surfaces.

In order to avoid fast drilling, both targets were placed on a vacuum-compatible computer controlled *XY* table. The

[a]Author to whom correspondence should be addressed; electronic mail: egyorgy@icmab.es
[b]Also at the Department of Chemical Engineering, National Technical University of Athens, 15780 Zografou, Athens, Greece.

 

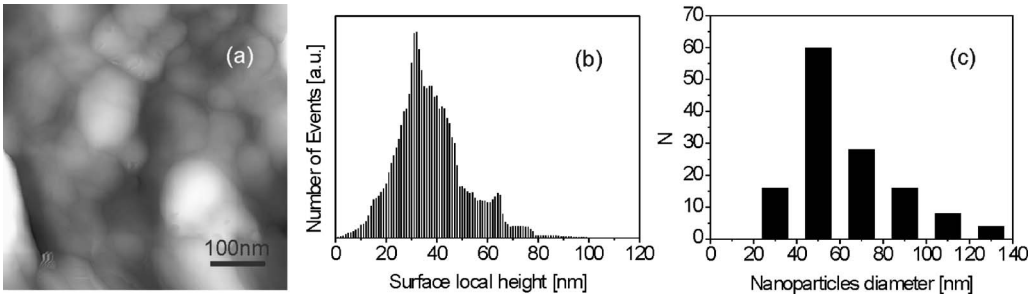


FIG. 1. (a) AFM images, (b) surface local height, and (c) particle diameter histograms counted on $0.5\times0.5$ $\mu m^2$ surface areas of the Au–$TiO_2$ nanostructured thin film deposited at 30 Pa oxygen pressure, 300 °C substrate temperature, and 7 $J/cm^2$ laser fluence incident on the Au target.

$SiO_2$ (001) quartz substrates were positioned 40 mm from the targets, where the two ablation plasmas intersect each other under an angle of 30°. The substrates were heated during the thin film growth at 300 °C. The depositions were performed in 30 Pa oxygen pressure. The $ArF^*$ laser fluence was 3 $J/cm^2$. The Nd:YAG laser fluence was fixed at values within the range of 1–7 $J/cm^2$. For the deposition of each film, we applied 21 000 laser pulses to both the $TiO_2$ and Au targets.

The surface morphology of the deposited films was studied by atomic force microscopy (AFM) with a PicoSPM Molecular Imaging apparatus. The morphology of the deposited films was also investigated by transmission electron microscopy (TEM) with JEOL 1210 equipment operated at 200 keV. The preparation of samples for TEM studies was carried out by the extraction replica method. The crystalline status was investigated by x-ray diffraction (XRD) in a $\theta$-$2\theta$ configuration with a Philips MRD diffractometer (Cu $K\alpha$, $\lambda=1.5418$ Å radiation) and selected area electron diffraction (SAED). The optical absorbance measurements were performed with a double beam Perkin Elmer Lambda 19 spectrophotometer in the wavelength range of 200–1000 nm.

## III. RESULTS AND DISCUSSION

### A. Morphological and structural properties

Figure 1 shows (a) a typical AFM micrograph, (b) surface local height, (c) and diameter histograms counted on $0.5\times0.5$ $\mu m^2$ areas of the thin film deposited with the highest, 7 $J/cm^2$ Nd:YAG laser fluence incident on the Au target. As can be observed, the film surface is characterized by a granular structure. The surface local height histogram consist of a double Gaussian distribution. The average height is approximately 40 nm for the main Gaussian and approximately 80 nm for the second Gaussian, which includes much less data points. From the nanoparticle diameter histogram we can estimate an average grain diameter of approximately 70 nm. We note that there are no significant differences between the surface features of the Ar–$TiO_2$ nanostructures obtained with the different laser fluences used for irradiation of the Au targets.

The bright field TEM investigations [Fig. 2(a)] made it clear that the thin films are composed of nanoparticles, but with much smaller dimensions when compared to AFM results. The histogram of the particle diameters shows an average size of about 30 nm (Fig. 3). This discrepancy can be explained by the influence of the AFM tip on the measurements. In order to reduce the widening effect which is more pronounced in the measurement of particle diameters, compared to height, we used a geometric deconvolution[18] and considered a spherical tip with a radius of 15 nm. The mean particle diameter after deconvolution is then approximately 40 nm, still slightly overestimated as compared to the TEM results. Conversely, as known, the surface height derived from AFM measurements is much less distorted by the AFM tip as compared to in-plane diameters.[19]

Indexing the SAED [Figs. 2(b) and 2(c)] patterns corresponding to selected zones, we obtain interplanar distances of 0.352 nm assigned to the (101) lattice plane reflection of the tetragonal anatase $TiO_2$ phase as referred to in the JCPDS Card No. 21-1272, and 0.235, 0.203, 0.117, and 0.101 nm attributed to the (111), (200), (222), and (400) lattice plane

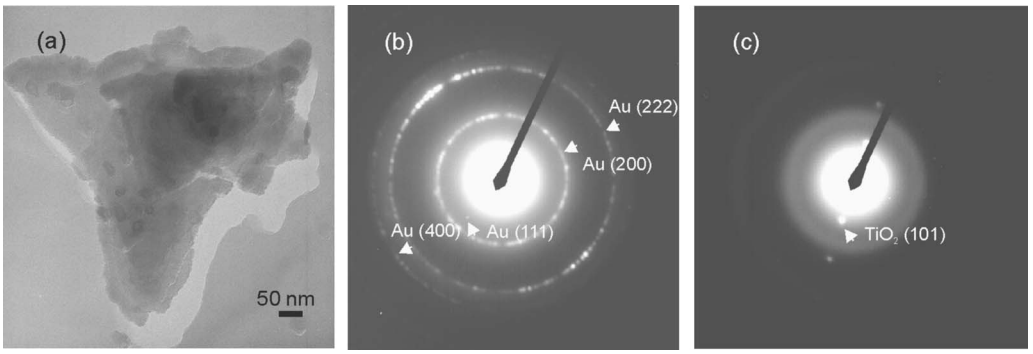


FIG. 2. (a) TEM image and [(b) and (c)] corresponding SAED patterns of the Au–$TiO_2$ nanostructured thin film deposited at 30 Pa oxygen pressure and 300 °C substrate temperature obtained with 2.3 $J/cm^2$ applied to the Au target.

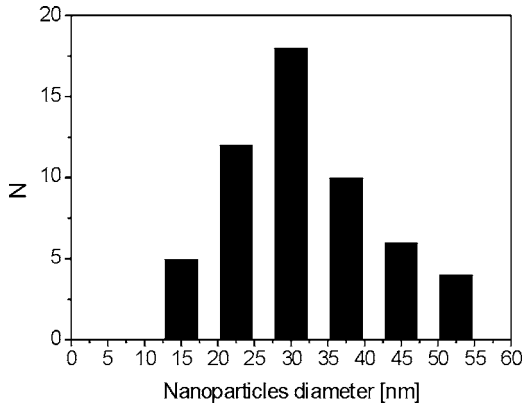


FIG. 3. Nanoparticle diameter histogram evaluated from TEM images of the Au–$TiO_2$ nanostructured thin film deposited at 30 Pa oxygen pressure and 300 °C substrate temperature obtained with 2.3 J/cm$^2$ laser fluence incident on the Au target.

reflection of the polycrystalline cubic Au phase, respectively, as referred to in the JCPDS Card No. 04-0784.[20] As can be observed, the diffraction rings are discontinuous and consist of sharp spots, indicating that the Au nanoparticles are well crystallized [Fig. 2(b)]. On the other hand, the $TiO_2$ matrix is formed by nanocrystals with the same growth orientation, with monocrystalline diffraction characteristics [Fig. 2(c)].

In order to obtain a complete view, the crystalline structure of the synthesized thin films was also investigated by XRD (Fig. 4). The diffractogram of the undoped, reference $TiO_2$ thin film [Fig. 4(a)] contains, besides the line assigned to the $SiO_2$ substrate, only one weak line at 25.3° attributed to the (101) lattice plane reflection of the tetragonal anatase $TiO_2$ phase, confirming the preferential growth orientation.[20] The diffractograms of the Au–$TiO_2$ nanostructures obtained with laser fluence below 2 J/cm$^2$ used for ablation of the Au targets are similar to those of the reference thin film [Fig. 4(b)]. The diffractogram of the nanostructures obtained with

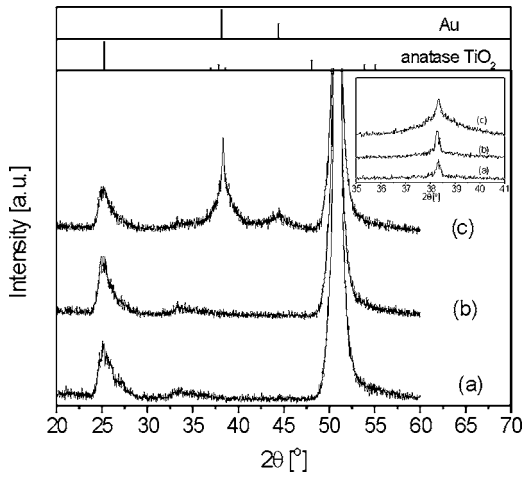


FIG. 4. XRD diffractograms of thin films deposited at 30 Pa oxygen pressure and 300 °C substrate temperature: (a) reference $TiO_2$ thin films and Au–$TiO_2$ nanostructured thin films obtained with (b) 1.2 and (c) 7 J/cm$^2$ laser fluence incident on the Au targets. The insert shows the (111) lattice place reflection of Au, for the Au–$TiO_2$ thin films obtained with (a) 2.3, (b) 3.2, and (c) 7 J/cm$^2$ laser fluence incident on the Au targets. The diffraction patterns of tetragonal anatase phase $TiO_2$, and cubic phase Au as referred to in the JCPDS Card No. 21-1272 and 04-0784 are also represented.

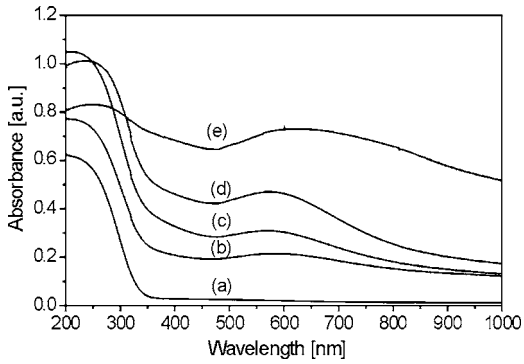


FIG. 5. UV-visible absorbance spectra of thin films deposited at 30 Pa oxygen pressure and 300 °C substrate temperature: (a) reference $TiO_2$ thin films and Au–$TiO_2$ nanostructured thin films obtained with (b) 1, (c) 2.3, (d) 3.2, and (d) 7 J/cm$^2$ laser fluence incident on the Au targets.

higher laser fluences applied to the Au targets [Fig. 4(c)] contains, besides the line at 25.3° of the anatase phase $TiO_2$, two new lines at 38.3° and 44.5° corresponding to the (111) and (200) lattice plane reflections of the cubic phase Au, respectively.[20] The insert shows the (111) lines of Au for the Au–$TiO_2$ nanocomposite films obtained with laser fluences higher than 2 J/cm$^2$. The intensity of the line increases with the increase of laser fluence, while the full width at half maximum (FWHM) remains approximately the same, about 0.37°. Applying Scherrer's equation to estimate the average Au particle size $R$, FWHM$=0.94\lambda/R\cos\theta$,[21] where $\lambda$ is the x-ray wavelength and $\theta$ is the diffraction angle, we obtain particle sizes of about 25 nm, in good agreement with TEM results.

### B. Optical properties

The typical optical absorption spectra of the reference $TiO_2$ thin film and the Au–$TiO_2$ nanostructures are shown in Fig. 5. With the increase of the laser fluence incident on the Au targets the optical characteristics of the Au–$TiO_2$ nanostructures gradually change in the UV-visible spectral range from transparent [Fig. 5(a)], in the case of the undoped $TiO_2$ film, to highly absorbent [Fig. 5(e)] for the highest laser fluence. In addition, in the spectra of the Au–$TiO_2$ nanostructures there is an absorption maximum centered at around 560 nm which appears even for the lowest Au concentration [Fig. 5(b)]. As can be observed, the intensity of this band increases with the increase of the laser fluence incident on the Au target, i.e., the increase of the amount of Au in the deposited thin films. The increase of the band intensity is accompanied by its continuous broadening. Neither significant band shift nor broadening could be observed, with the exemption of the spectrum corresponding to the nanocomposite film obtained with the highest laser pulse energy [Fig. 5(e)].

The absorption maximum around 560 nm is associated with the surface plasmon resonance (SPR) absorption band of individual Au nanoparticles.[22] As is well known, the main changes in the surface plasmon resonance band characteristics are related to the noble metal nanoparticle size,[22,23] shape,[24] or their volume fraction (nanoparticles embedded in a ceramic matrix) in the case of nanocomposite thin films.[25]

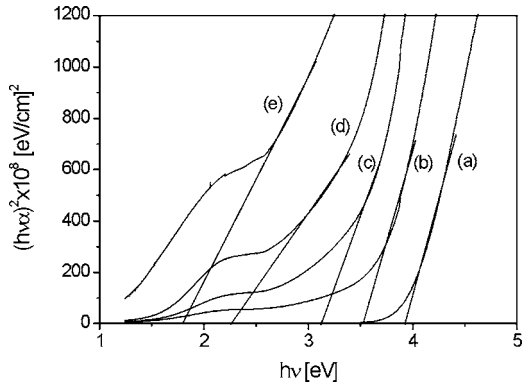


FIG. 6. Plot of $(h\nu\alpha)^2$ vs $h\nu$ for thin films deposited at 30 Pa oxygen pressure and 300 °C substrate temperature: (a) reference $TiO_2$ thin films and $Au-TiO_2$ nanostructured thin films obtained with (b) 1, (c) 2.3, (d) 3.2, and (d) 7 $J/cm^2$ laser fluence incident on the Au targets.

As a general rule the absorption band's intensity increases with the increase of the number of nanoparticles. Its broadening and shift towards higher wavelengths are caused by the increase of the nanoparticle size.

Thus, the gradual increase of the intensity of the SPR absorption band with the increase of the incident laser fluence could be due to the increase of the Au nanoparticle concentration. Furthermore, the shift of the absorption band towards higher wavelength (to approximately 650 nm) could indicate both an increase of Au nanoparticle dimensions and the formation of nanoparticle aggregates. However, no significant increase of grain size could be observed through XRD investigations. Thus, the observed absorption features could be caused only by coalescence of the Au nanoparticles with the increase of their density in the $TiO_2$ matrix.

As can also be observed, the absorption edge of the reference $TiO_2$ thin film [Fig. 5(a)] is shifted towards smaller wavelengths as compared with the band gap of bulk $TiO_2$ (3.2 eV at 388 nm). This shift could be attributed to quantum confinement effect induced both by crystallites with low sizes[26] and/or residual stress in the films exerted by the substrate.[27] The absorption edge is displaced towards lower photon energies with the increase of the incident laser fluence, i.e. the increase of the amount of Au in the deposited $Au-TiO_2$ nanostructures [Figs. 5(b)–5(e)].

The measured absorbance was converted into absorption coefficient using the relationship $\alpha=(A \ln 10)/d$, where $d$ is the thickness of the films. From cross-sectional scanning electron microscopy (SEM) investigations a thickness value of about 200 nm was determined. Figure 6 shows the behavior of $(h\nu\alpha)^2$ as a function of photon energy. The band gap values were estimated from the dependence $(h\nu\alpha)^2 \sim (E-E_g)$ at the interception of the tangents to the $(h\nu\alpha)^2$ plots with the photon energy axis.[28] The band gap narrowing with the increase of the laser fluence could be due to the incorporation of Au into the $TiO_2$ lattice.[29] Similar results have been obtained in the case of the $Au-CeO_2$ system, as a class of oxidation catalysts.[30]

The continuous bandgap narrowing and increasing additional SPR absorption with the increase of Au incorporated into the matrix ensure the creation of $Au-TiO_2$ composite systems with tunable optical properties both in the near-UV and visible spectral ranges. The established dependence between the laser fluence used for the ablation of the Au targets and absorption characteristics allows the growth of $Au-TiO_2$ nanostructures with predetermined optical properties for photocatalysts and solar energy converters.

## IV. CONCLUSIONS

Anatase phase $TiO_2$ films and $Au-TiO_2$ nanostructures were grown by pulsed laser deposition on quartz substrates with the aid of a dual-laser, dual-target system. We studied the correspondence between the laser irradiation parameters (e.g., laser fluence used for the irradiation of the Au targets) and optical properties of $Au-TiO_2$ nanostructures. We have shown that there exists the possibility of the controlled tailoring of the optical properties of the nanostructure systems in the near-UV and visible spectral regions. Our results evidenced that through the control of growth parameters we can achieve both continuous band gap narrowing as compared to the undoped $TiO_2$ thin films in the near-UV and tuning of the SPR peak in the visible spectral range. These features promise a wide range of applications, overcoming the main drawback of undoped $TiO_2$ absorbing only in the UV region.

## ACKNOWLEDGMENTS

Financial support by NATO (PST.CLG 980464) and Generalitat de Catalunya (OTT-2005-X-1070) is acknowledged. One of the authors (A.G.) thanks the Hellenic General Secretariat for Research and Technology for partial financial support through a bilateral Greek-Slovakian 2004-06 Research Agreement.

[1] N. Ruzycki, G. S. Herman, L. A. Boatner, and U. Diebold, Surf. Sci. Lett. **529**, L239 (2003).
[2] A. Fujishima, T. N. Rao, and D. A. Tryk, J. Photochem. Photobiol. C **1**, 1 (2000).
[3] R. Asahi, T. Morikawa, T. Ohwaki, K. Aoki, and Y. Taga, Science **293**, 269 (2001).
[4] M. Anpo, Pure Appl. Chem. **72**, 1265 (2000).
[5] I. M. Arabatzis, T. Stergiopoulos, M. C. Bernard, D. Labou, S. G. Neophytides, and P. Falaras, Appl. Catal., B **42**, 187 (2003).
[6] J. Yu, J. Xiong, B. Cheng, and S. Liu, Appl. Catal., B **60**, 211 (2005).
[7] M. I. Litter, Appl. Catal., B **23**, 89 (1999).
[8] D. Hufschmidt, D. Bahnemann, J. J. Testa, C. A. Emilio, and M. I. Litter, J. Photochem. Photobiol., A **148**, 223 (2002).
[9] I. Justicia, P. Ordejon, G. Canto, J. L. Mozos, J. Fraxedas, G. A. Battiston, R. Gerbasi, and A. Figueras, Adv. Mater. (Weinheim, Ger.) **14**, 1399 (2002).
[10] S. Ben Amor, L. Guedri, G. Baud, M. Jacquet, and M. Ghedira, Mater. Chem. Phys. **77**, 903 (2002).
[11] Y. Q. Hou, D. M. Zhuang, G. Zhang, M. Zhao, and M. S. Wu, Appl. Surf. Sci. **218**, 97 (2003).
[12] U. Cernigoj, U. L. Stangar, P. Trebse, U. O. Krasovec, and S. Gross, Thin Solid Films **495**, 327 (2006).
[13] I. Saeki, N. Okushi, H. Konno, and R. Furuichi, J. Electrochem. Soc. **143**, 2226 (1996).
[14] A. A. Gorbunov, H. Eichler, W. Pompe, and B. Huey, Appl. Phys. Lett. **69**, 2816 (1996).
[15] T. Nakamura, T. Ichitsubo, E. Matsubara, A. Muramatsu, N. Sato, and H. Takahashi, Acta Mater. **53**, 323 (2005).
[16] H. Matsui, H. Tabata, N. Hasuike, H. Harima, and B. Mizobuchi, J. Appl. Phys. **97**, 123511 (2005).
[17] E. György, G. Socol, E. Axente, I. N. Mihailescu, C. Ducu, and S. Ciuca, Appl. Surf. Sci. **247**, 429 (2005).
[18] D. Keller, Surf. Sci. **253**, 353 (1991).
[19] J. C. Hulteen, D. A. Treichel, M. T. Smith, M. L. Duval, T. R. Jensen, and

R. P. Van Duyne, J. Phys. Chem. B **103**, 3854 (1999).
[20]JCPDS-International Center for Diffraction Data Card No. 21-1272, 1986 (Unpublished); JCPDS-International Center for Diffraction Data Card No. 09-0789, 1986 (Unpublished).
[21]B. D. Cullity, *Elements of X-ray Diffraction*, 2nd ed. (Addison-Wesley, London, 1978).
[22]U. Kreibig and M. Vollmer, *Optical Properties of Metal Clusters* (Springer, Berlin, 1995).
[23]D. M. Schaadt, B. Feng, and E. T. Yu, Appl. Phys. Lett. **86**, 063106 (2005).
[24]S. Chakrabarti, D. Ganguli, and S. Chaudhuri, Mater. Lett. **58**, 3952 (2004).
[25]S. Hazra, A. Gibaud, and C. Sella, Appl. Phys. Lett. **85**, 395 (2004).
[26]M. I. Freedhoff and A. P. Marchetti, in *Handbook of Optical Properties: Optics of Small Particles, Interfaces, and Structures*, edited by R. E. Hummel and P. Wissman (CRC, New York, 1997), Vol. II, pp. 1–30.
[27]Y. Du, M. S. Zhang, J. Wu, L. Kang, S. Yang, P. Wu, and Z. Yin, Appl. Phys. A: Mater. Sci. Process. **76**, 1105 (2003).
[28]J. Tauc, in *Amorphous and Liquid Semiconductors*, edited by J. Tauc (Plenum, New York, 1974), pp. 159–220.
[29]S. Chretien and H. Metiu, Catal. Lett. **107**, 143 (2006).
[30]Q. Fu, H. Saltsburg, and M. Flytzani-Stehanopoulos, Science **301**, 935 (2003).